IEEE Access
Multidisciplinary | Rapid Review | Open Access Journal

Received June 30, 2021, accepted September 4, 2021, date of publication September 29, 2021,
date of current version October 5, 2021.

Digital Object Identifier 10.1109/ACCESS.2021.3116282

Detection of Corrosion in Thick Film Resistors by X-Ray Imaging

JONNY M. INGMAN[1,2], (Graduate Student Member, IEEE), JONI P. A. JORMANAINEN[1], SAMU K. JÄRVINEN[1], NATALIA I. KANKO[1], JOONAS A. R. LEPPÄNEN[1], ALEKSI M. VULLI[1], TOMMI J. KÄRKKÄINEN[2], (Member, IEEE), JUUSO RAUTIO[2], (Member, IEEE), JANNE JÄPPINEN[2], (Member, IEEE), AND PERTTI SILVENTOINEN[2], (Member, IEEE)

[1]ABB Oy, 00381 Helsinki, Finland
[2]LUT School of Energy Systems, LUT University, 53851 Lappeenranta, Finland

Corresponding author: Jonny M. Ingman (jonny.ingman@fi.abb.com)

ABSTRACT In this article, a non-destructive method is presented, using 2D X-ray imaging, to investigate corrosion defects in thick film resistors stressed by two different corrosion experiments, a single gas experiment and a flowers of sulphur experiment. In total, 370 devices under test (DUTs) were investigated, using the 2D X-ray imaging technique, of which 10 were imaged in a sequence of 2D X-ray images to evaluate the corrosion propagation. The observed underlying corrosion product was verified by using focused ion beam analysis combined with an energy dispersive X-ray spectroscopy. The presented 2D X-ray imaging technique enables a fast and non-destructive method for accurately identifying corrosion and corrosion progression in thick film resistors. The presented imaging method was found to be particularly suitable for supplier benchmarking purposes, as well as for the failure analysis of field returns as it allows for a proper corrosion evaluation of surface mount thick film resistors, while keeping the analysed assembly intact.

INDEX TERMS Corrosion, resistors, failure analysis, scanning electron microscopy, silver, sulphur, X-rays.

I. INTRODUCTION

Frequency converters are used in vastly different fields of industries and applications, such as solar, wind, pulp and paper production, rubber vulcanization and mining. In solar applications, one of the biggest stressors for a frequency converter is temperature cycling, which has a big impact on the ageing phenomena of the insulated gate bipolar transistor (IGBT). In wind applications, humidity plays a significant role on the drive's reliability. Other harsh environments, such that contains corrosive pollutants, can be found in pulp and paper production, as well as in rubber vulcanization and mining applications. In these industries, the amount of atmospheric sulphur in the environment has a big impact on the lifetime of the frequency converter. Critical components, such as power modules [1], electrical contacts and thick film resistors are affected by corrosion due to sulphur in the environment. In these electrical components, corrosion phenomena, such as electrochemical migration [1]–[3] and open connection [4], [5], have been reported.

The associate editor coordinating the review of this manuscript and approving it for publication was Zeev Zalevsky.

Surface mount thick film resistors are used in almost all industrial electronic devices. Although the resistor is one of the simplest and most inexpensive amongst all of the other components, it may be responsible for the complete functional breakdown of a device operating in a harsh environment. In these environments, corrosion failures such as resistive shorts, open connections or changes in resistance indicating intermittent failure are typical. Usually, in sulphuric atmospheres, the weakest spot in a thick film resistor is the silver (Ag) termination. It is well known that silver can rapidly corrode in harsh atmospheres, particularly in those containing sulphides [6]–[8]. Silver reacts with sulphur (S), forming silver sulphide (Ag_2S). Silver sulphide is known to be non-conductive and leads to changes in resistance or, eventually, an open circuit [4]. This silver termination is the most underlying layer in the resistor structure. It is protected by two different metallic terminations. The first one is a protective barrier, typically made of nickel (Ni), and the second one is an outer solder termination of tin (Sn). Additionally, a thin conformal organic epoxy layer is applied to the resistor to limit the gas permeation of water vapour and pollutant gases to reach the silver termination. A typical cross-section

image of a thick film resistor is shown in Fig. 1a) with the corresponding areas of interest visualized in Fig. 1b).

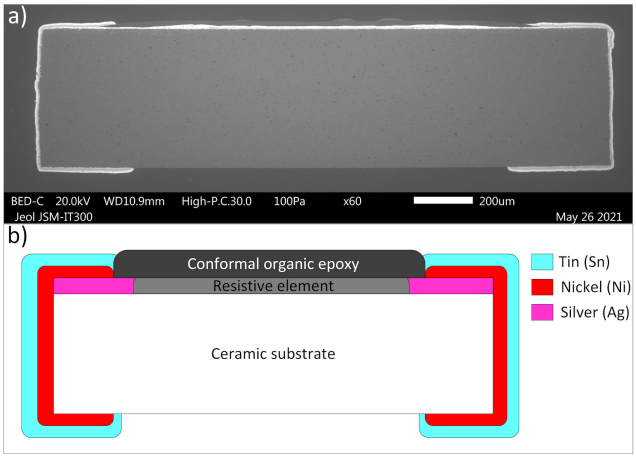

FIGURE 1. a) Scanning electron microscope image of a typical cross-sectioned thick film resistor. b) an illustrated image of the different materials and layers used in a thick film resistor.

Many different corrosion tests have been utilized to investigate the behaviour between the thick film resistor and the corrosive sulphur. Typical corrosion tests are single gas [9]–[11] and flowers of sulphur (FoS) [11]–[13] tests. In single gas tests, the thick film resistors are exposed to a high level of hydrogen sulphur (H_2S) or sulphur dioxide (SO_2) at a high temperature and high humidity. The corrosive gas concentration in these tests have varied from 1 – 10 ppm and 1 – 15 ppm, respectively [14], [15]. Flowers of sulphur test is one of the simplest corrosion tests when compared to other gaseous experiment setups. In this test, sulphuric powder is held at the bottom of a desiccator and the thick film resistors hang above the sulphur powder. No humidity is used, instead, a high temperature is applied. Usually, the thick film resistors are tested without voltage in these corrosion experiments and no information is presented in the literature where thick film resistors have been exposed to both corrosive gas and electrical stress.

The failure mechanism for thick film resistors in a sulphuric atmosphere is a chemical reaction between the silver termination and the sulphur. The reaction between silver and sulphur causes the electrical connection to be non-conductive and, eventually, leads to an open circuit. Typically, cross-sections of the DUTs have been done to determinate the existence of non-conductive silver sulphide corrosion. One of the major drawbacks with this analysis method is that it is destructive, and, therefore, the propagation of the corrosion in a thick film resistor has not been properly investigated. Also, in previous studies [9]–[12] optical and scanning electron microscopy imaging methods have been utilized for analysing the corrosion on the surface of a thick film resistor. The drawback with these imaging techniques is that the underlying corroded silver layer is not visible, and the magnitude of the corrosion has not been fully determined.

This study demonstrates an effective non-destructive X-ray imaging method for analysing corrosion in thick film resistors. Multiple studies [16]–[20] have shown successful results of analysing corrosion by X-ray imaging, where stainless steel and steel used in concrete have been analysed. In our study, standard commercial thick film resistors from different vendors were subjected to sulphuric atmosphere in two different corrosion experiment setups: single gas and flowers of sulphur. In each of the experiment setups, 90 resistors were electrically stressed, and 90 resistors were unbiased. A data acquisition (DAQ) unit was used to continuously measure the voltages and resistances of the DUTs during the experiments in order to observe any corrosion propagation. 2D X-ray imaging was implemented to provide deeper insight for assessing the propagation of the corrosion. Large differences in the resistors' corrosion behaviour were observed between the vendors and between the experiment systems. It was also found that with X-ray imaging it was possible to detect the corrosion before it was observed in the electrical measurements.

II. METHODS

A. EXPERIMENT SETUPS

Two experiment setups, a flowers of sulphur (FOS) experiment and a single gas experiment, were designed and built to induce corrosion in standard commercial thick film resistors. For both corrosions experiments, standards related to corrosion testing were followed. For the flowers of sulphur experiment, the EIA-977 [21] standard was followed. The single gas experiment was carried out based on IEC 60068-2-43 [14], with increased temperature and humidity to accelerate the corrosion.

Thick film resistors used as DUTs were soldered onto printed circuit boards (PCBs) specifically designed for the experiment. Experiments were carried out in both biased (Fig. 2a) and unbiased (Fig. 2b) configurations. Each PCB can hold up to 100 thick film resistors of which 90 (R1 to R90 in Fig. 2) in 9 groups of 10 resistors each were connected in parallel to its own PCB power supply terminals. Thus, 9 different vendors could be easily tested per test board. All thick film resistors were mounted with a 96.5 Sn - 3.0 Ag - 0.5 Cu solder and all had resistance values of 4700 Ω with a rated voltage of 150 V. The package size used was a standard 0805 package in all experiments and the electrical and structural specifications of the analysed thick film resistors are given in Table 1. The measured values in Table 1 were obtained with SEM and EDX.

For the FOS experiment, 2 boards were used with both having resistors from 9 different vendors. For each vendor, 10 thick film resistors were connected in parallel resulting in 90 DUTs in total per board. To assess the influence of voltage bias on the corrosion of the resistors, the first board was unbiased, and the second board was biased with a voltage of 10 V resulting in 2.5 V over the reference resistors and 7.5V over the DUTs. For the unbiased board, the parallel resistance values of the 9 resistor groups were measured

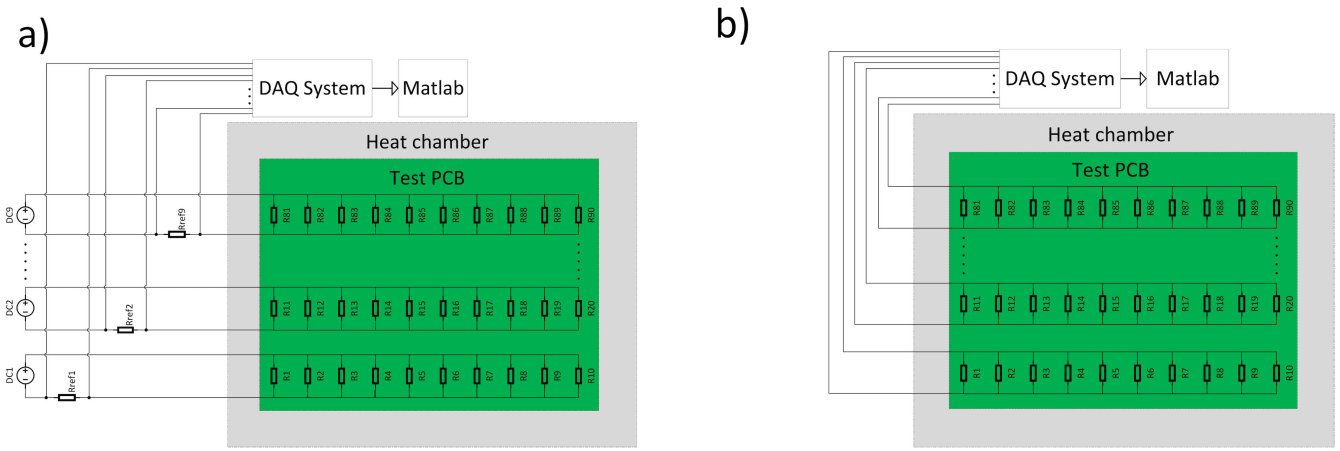

FIGURE 2. Schematic diagrams of both test setups. a) voltage biased experiment setup and b) unbiased experiment setup.

TABLE 1. The electrical (from datasheet) and structural (measured) specifications of the DUTs.

	Datasheet values							Measured values			
Supplier	Package type	Package	Max. dissipation (mW)	Temperature range (°C)	Max operation voltage (V)	Resistance tolerance	Resistance (Ω)	Epoxy thickness	Plating	Protective metallization	Inner electrode
A	Standard	0805	125	-55 to +155	150	1 %, 100 ppm	4700	$\leq 1\,\mu$m	Sn	Ni	Ag
B	AS[1]	0805	125	-55 to +155	150	1 %, 100 ppm	4700	$10.8\,\mu$m	Sn	Ni	Ag
C	Standard	0805	125	-55 to +155	150	1 %, 100 ppm	4700	$3.1\,\mu$m	Sn	Ni	Ag
D	Standard	0805	125	-55 to +155	150	1 %, 100 ppm	4700	$4.5\,\mu$m	Sn	Ni	Ag
E	Standard	0805	125	-55 to +155	150	1 %, 100 ppm	4700	$\leq 1\,\mu$m	Sn	Ni	Ag
F	Standard	0805	125	-55 to +155	150	1 %, 100 ppm	4700	$5.7\,\mu$m	Sn	Ni	Ag
G	Standard	0805	125	-55 to +155	150	1 %, 100 ppm	4700	$12.4\,\mu$m	Sn	Ni	Ag
H	Standard	0805	125	-55 to +155	150	1 %, 100 ppm	4700	$5.2\,\mu$m	Sn	Ni	Ag
I	Standard	0805	125	-55 to +155	150	1 %, 100 ppm	4700	$16.6\,\mu$m	Sn	Ni	Ag

[1] Anti-sulfur

TABLE 2. Test specifications of each corrosion experiment.

Experiment	Corrosive substance	Voltage Bias (V)	Temperature (°C)	Relative Humidity (%)	Number of DUTs	Test Duration (h)
Flowers of Sulphur	Sulphur powder	0	105	-	90	750
Flowers of Sulphur	Sulphur powder	7.5	105	-	90	750
Flowers of Sulphur	Sulphur powder	0	105	-	10	200
Single Gas	H_2S gas	0	60	90	90	750
Single Gas	H_2S gas	7.5	60	90	90	750

directly with an Agilent 34970A data acquisition unit equipped with Agilent 34901A multiplexers. For the biased board, the voltage over an external 160 Ω reference resistor outside the chamber, one per resistor group, was measured to electrically verify the propagation of the corrosion in the DUTs. In an event of a resistor open circuit, the change in voltage and/or resistance was recorded by the DAQ unit to enable a time-to-failure comparison between the different vendors. An additional unbiased FOS experiment was performed by using 10 DUTs of only one supplier where each resistance value of each single resistor was measured directly. In this experiment, X-ray images of the DUTs were obtained every 12h to analyse the corrosion propagation.

In the flowers of sulphur experiment, sulphuric powder CAS:7704-34-9 was used. The powder was placed in a petri dish and set at the bottom of a desiccator. Two desiccators were used in this experiment, one for the unbiased DUTs and one for the biased. Both desiccators were kept in a heat chamber at 105 °C for 750 hours, as specified in [21].

The single gas experiment was performed similarly as described for the FOS experiment, except no additional unbiased experiment with single resistors were performed. In the single gas experiment, the test PCBs were mounted inside a glass vessel placed inside a heat chamber. The temperature in the experiment (inside the heat chamber) was set to 60 °C, the relative humidity was set to 90 % and controlled with a separate vessel by a mixture of air and 68 °C water. The H_2S-concentration of 15 ppm was adjusted by a mixing of dry air and a bottled gas of nitrogen with 500 ppm H_2S using a mass balance meter and a rotameter. The total gas flow was adjusted to 3 l/min and a Dräger X-am 5000 gas detector was used to measure the H_2S concentration during the experiment. An illustrative drawing of the single gas experiment setup is shown in Fig. 3 and Table 2 presents the corrosion experiment specifications of each experiment.

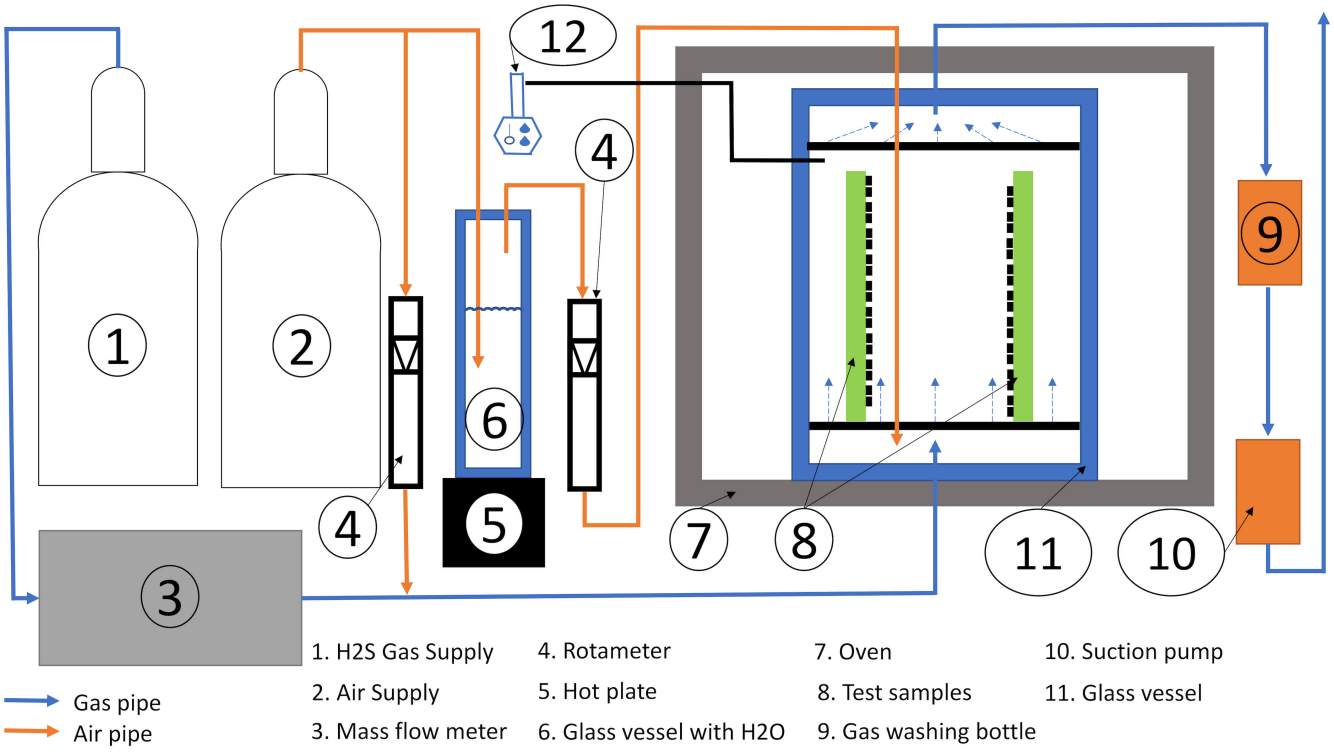

FIGURE 3. A schematic picture of the single gas experiment.

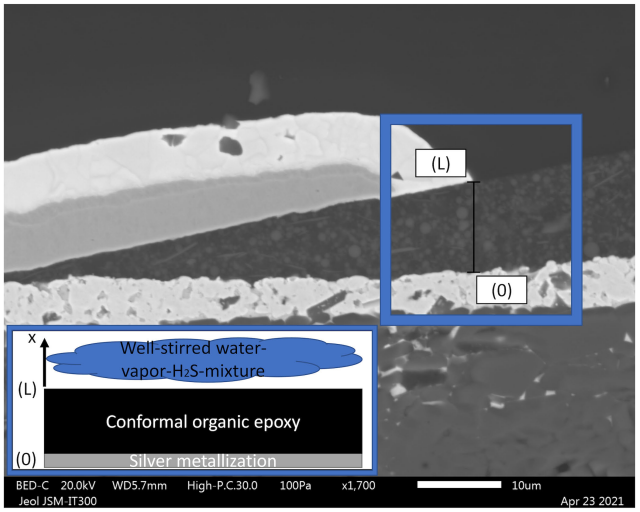

FIGURE 4. An illustrated image of the diffusion through the conformal epoxy layer.

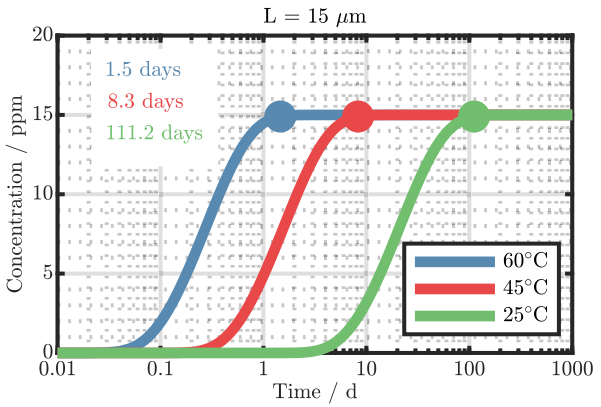

FIGURE 5. H_2S diffusion through conformal organic epoxy layer in thick film resistors in different temperatures.

B. STANDARDS RELATED TO CORROSIVE GAS TESTING

In the single gas experiment the temperature influences the diffusion of water vapor and H_2S gas through the conformal organic epoxy layer. The corrosion does not commence before the gas mixture encounters the underlying silver metallization. Therefore, to define a suitable temperature for the single gas experiment, a diffusion model in a theoretical setting is described in Fig. 5. Here, the surface of the epoxy at $x = L$ is exposed to a well-stirred water-vapor-H_2S-mixture imposing one-dimensional mass diffusion in the x-direction, through the epoxy to the silver metallization at $x = 0$. The following assumptions apply:

- no chemical interactions occur,
- the temperature is uniform in all layers and
- the mass transfer between the epoxy and the silver metallization at $x = 0$ is negligible,

whereby the mass transfer within the epoxy is expressed as [22, p. 889]

$$\frac{\partial^2 C}{\partial x^2} = \frac{1}{D}\frac{\partial C}{\partial t} \tag{1}$$

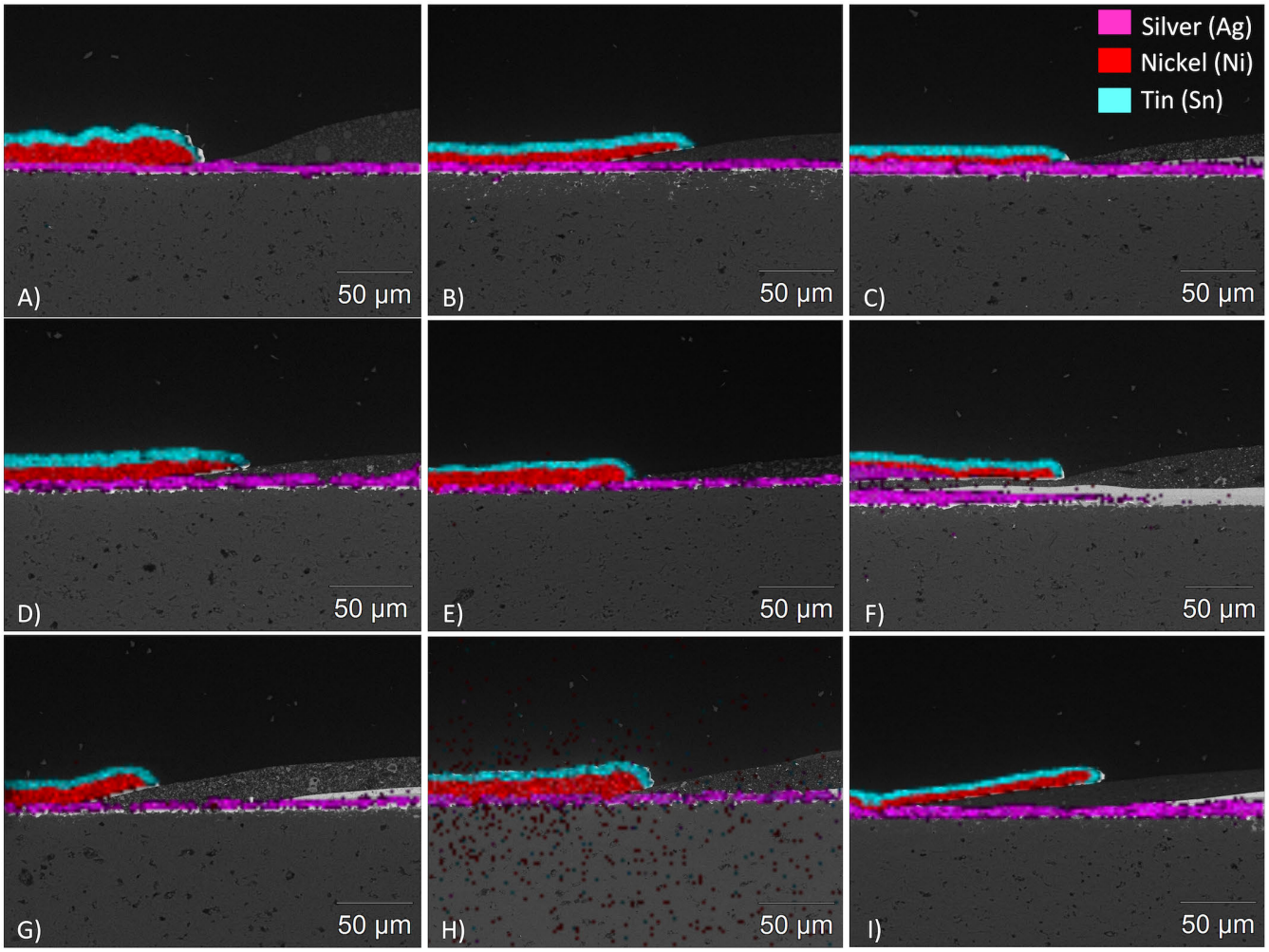

FIGURE 6. An energy dispersive X-ray spectroscopy mapping of the DUTs.

where C is the mass concentration in consistent units (ppm), x is the distance (m), D is the coefficient of diffusion (m^2/s) and t is the time (s). For the initial uniform concentration, the following assumption applies [22, p. 890]

$$C(x, 0) = C_i. \tag{2}$$

To solve the equation (1), the following boundary conditions are needed [22, p. 890]

$$\left.\frac{\partial C}{\partial x}\right|_{x=0} = 0 \tag{3}$$

$$C(L, t) = C_a \tag{4}$$

where L is the thickness of the conformal epoxy layer (m). An exact solution to the gas concentration at the metallic silver layer ($x = 0$) is of the form [22, p.257]

$$\frac{C(0,t) - C_a}{C_i - C_a} = \sum_{n=1,3,5}^{\infty} \sin\left(\frac{n\pi}{2}\right) \exp\left[-\left(\frac{n\pi}{2}\right)^2 \left(\frac{Dt}{L^2}\right)\right]. \tag{5}$$

TABLE 3. Physical properties for H_2S and H_2O [10].

Concentration	D_{REF} (m^2/s)	T_{REF} (K)	E_a (eV)
H_2S	$8.00 \cdot 10^{-13}$	340	1.060
H_2O	$1.53 \cdot 10^{-15}$	295	0.414

The effect of temperature was modelled as the Arrhenius relationship in the diffusion coefficient as [10]

$$D(T) = D_{\mathrm{REF}} \exp\left[-\frac{E_a}{\mathrm{k}}\left(\frac{1}{T} - \frac{1}{T_{\mathrm{REF}}}\right)\right], \tag{6}$$

where D_{REF} is the diffusion coefficient (m^2/s) at the reference temperature, E_a is the activation energy (eV), k is the Boltzmann's constant $8.617 \cdot 10^{-5}$ eV/K, T is the absolute temperature (K) and T_{REF} is the reference temperature (K). Table 3 presents the physical properties for H_2S and H_2O to calculate the theoretical diffusion through the conformal organic epoxy layer [10].

The temperature in the standard [14] for single gas experiments has been specified as $25\,^{\circ}\mathrm{C} \pm 2\,^{\circ}\mathrm{C}$. As can be seen

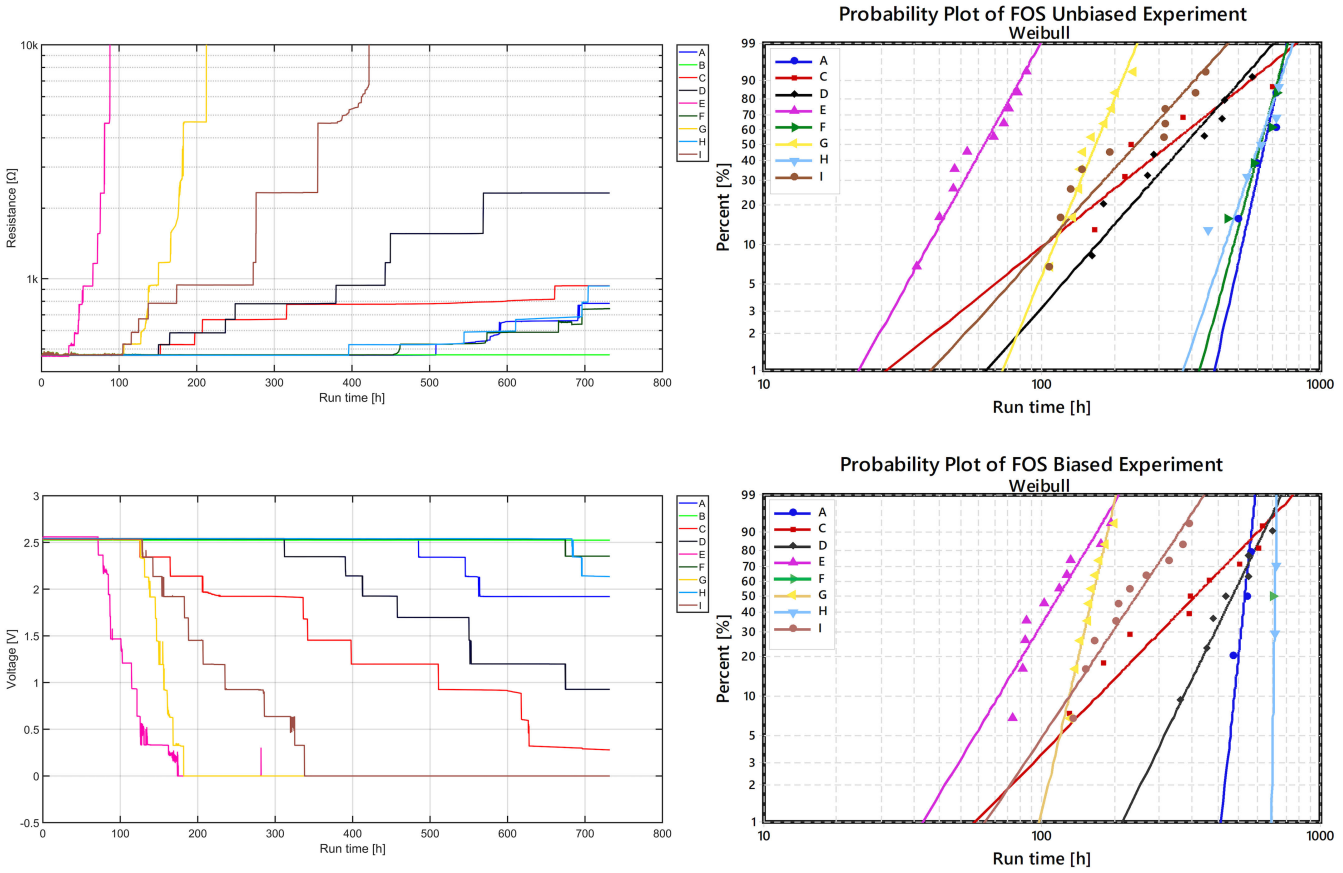

FIGURE 7. In-situ measurements of tested DUTs in un-biased and biased FOS experiment and corresponding time-to-failure probability plots.

TABLE 4. The obtained parameters from the Weibull probability distribution.

FOS Unbiased Experiment						FOS Biased Experiment					
Vendor	β	η	N	AD	p	Vendor	β	η	N	AD	p
A	10.14	655	4	0.44	0.241	A	21.71	545.7	3	0.349	>0.250
B	-	-	-	-	-	B	-	-	-	-	-
C	1.8	351.8	5	0.484	0.201	C	2.318	415	9	0.287	>0.250
D	2.568	374.7	8	0.326	>0.250	D	4.636	523.3	7	0.233	>0.250
E	4.066	67.47	10	0.311	>0.250	E	3.766	125.8	10	0.492	0.205
F	8.417	638.1	4	0.301	>0.250	F	-	-	1	-	-
G	5.489	166.3	10	0.293	>0.250	G	9.652	157.6	10	0.232	>0.250
H	6.725	635.8	5	0.34	>0.250	H	133.6	692.3	2	0.365	>0.250
I	2.488	252.1	10	0.52	0.178	I	3.371	243.1	10	0.346	>0.250

in Fig. 5 for the H_2S to reach the inner silver layer in the thick film resistors, it would take approximately 111 days to reach the level of 15 ppm H_2S. On the contrary, for a temperature of 60 °C it would take around 1.5 days. Therefore, it was not useful to perform a single gas experiment at the specified temperature as given in the standard [14]. It was also calculated that it takes four days for the H_2O to reach equilibrium at 60 °C. Wassermann *et al.* [1] have shown that increased humidity has an impact on the corrosion behaviour of electronics in a single gas testing, where a higher humidity generated larger dendrite structures under, otherwise, the same conditions. Therefore, a 90% relative humidity was chosen instead of 70% as specified in the standard [14].

C. ANALYSIS METHODS

X-ray images of the thick film resistors were obtained with an industrial Phoenix Nanomex X-ray machine, using both 2D and μ-computerized tomography (μ-CT) X-ray imaging technologies. For the scans, the maximum detail detectability of the open nanofocus x-ray tube was 200 nm [23].

In 2D X-ray imaging, a beam current of 150 μA and a voltage of 130 kV were used. All thick film resistors were imaged before and after the experiments to investigate the propagation of the corrosion. In μ-computerized tomography X-ray imaging, the DUTs were only imaged after the experiment since the DUTs needed to be cut out from the test PCBs to obtain high resolution images. In the μ-computer

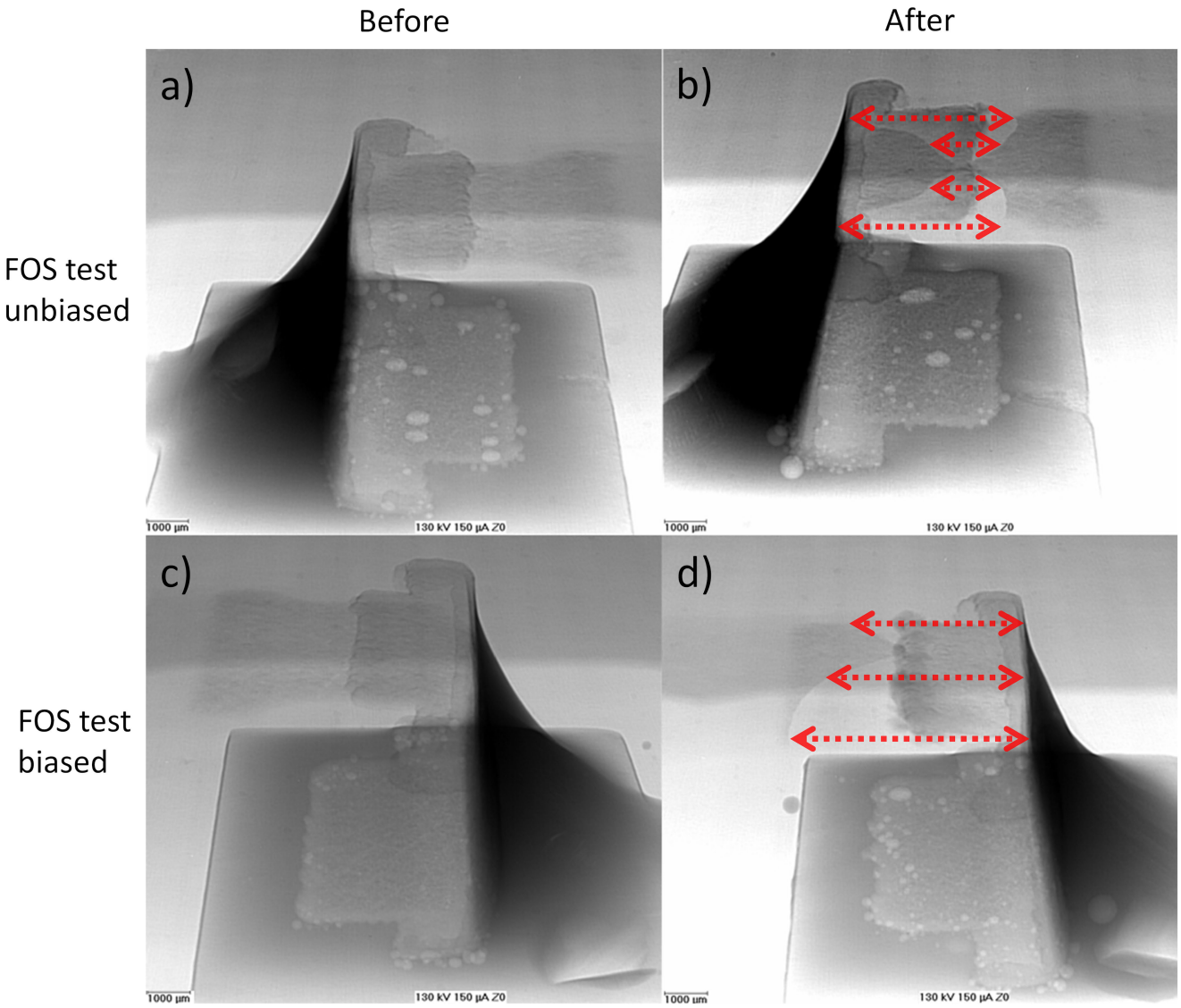

FIGURE 8. 2D X-ray images of both unbiased and biased DUTs (vendor D) taken before and after the FOS experiment. a) and c) images depicts the initial state of silver electrodes of the DUTs for both the unbiased and biased experiments, respectively. b) and d) depicts the corroded electrodes of two of the failed DUTs in the unbiased and biased FOS experiments, respectively.

tomography imaging, the DUTs were placed on a rotation stage between the radiation source and the flat panel detector. Each thick film resistor was rotated by 360° and 1200 2D X-ray images were taken. The images obtained were then reconstructed by using datos|x 2 and VGStudio MAX software into a 3D model that can be sliced into multiple virtual cross section images. The 3D model produced was utilized to analyse the structure of the corroded thick film resistor. This method has been shown to be successful in displaying miniscule defects in electronic components such as multilayer ceramic capacitors [24].

To analyse the materials used in the end termination for each supplier, cross-section preparation techniques were utilized. For the cross-sectioning, the DUTs were encapsulated into epoxy for structural support during the grinding. The exposed surface was ground gradually by using silicon carbide grinding papers with grain sizes ranging from P320 to P4000. The final polishing was made by using woven acetate polishing cloths and aluminium oxide polishing films combined with polycrystalline diamond lubricants at grain sizes of 9 μm, 3 μm and 1 μm. Furthermore, the DUTs were polished with a JEOL cross section polisher to obtain a contaminant free DUT after the grinding process by using argon gas for the polishing. The flow rate for the argon gas was adjusted to 6.2 and an acceleration voltage of 7.0 kV was used in this study. The polishing process for each DUT was adjusted to 45 minutes. After polishing, the results of each thick film resistor were captured with a JEOL JSM-IT300 scanning electron microscopy combined with a Thermofischer energy dispersive X-ray spectroscopy (EDX).

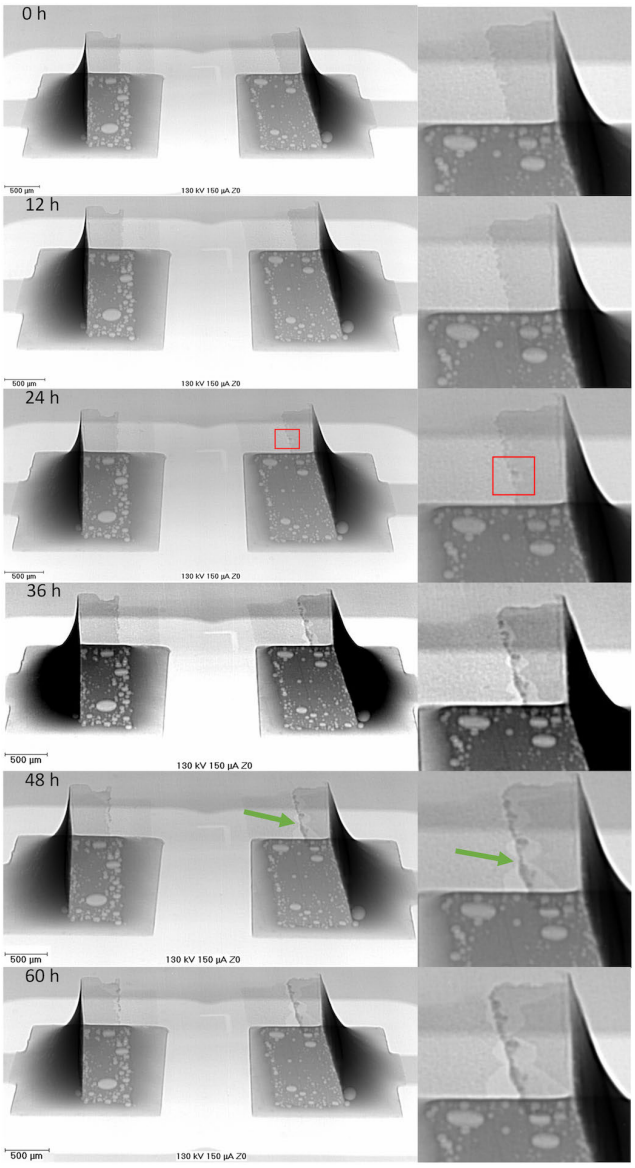

FIGURE 9. A sequence of X-ray images showing the corrosion propagation in thick film resistor (vendor E). The red box at 24 h indicates the first sign of corrosion and the green arrow at 48 h shows that only a small electrical connection is remaining.

To verify silver electrode corrosion in the thick film resistor DUTs, a JEOL JIB-4700F focused ion beam (FIB) with a gallium ion source was used. This technique allows for a contaminant free material identification of the inner structure of the analysed DUT. The final corrosion product was analysed by a JEOL energy dispersive X-ray spectroscopy.

III. RESULTS

A. STRUCTURAL INVESTIGATION

The thick film resistor end termination structure was investigated by cross-sectioning. All DUTs were ground and polished to the middle of the package. Fig. 6 shows an EDX and scanning electron microscopy image of each suppliers' end

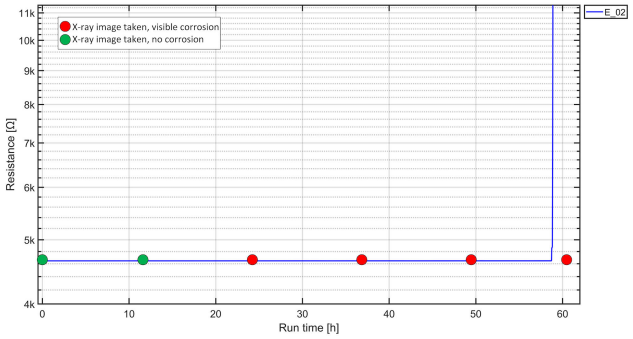

FIGURE 10. Online resistance measurement of a single DUT (vendor E).

termination structure after the polishing process. In all DUTs, tin and nickel were found in the top metallization and the protective barrier, respectively. Underneath the nickel layer, a silver layer was observed in all thick film resistors. The only difference between the suppliers was the thickness of the conformal organic epoxy layer.

B. TEST RESULTS

The time-to-failure (TTF) probability plot for the FOS experiment is shown in Fig. 7. The top row shows the TTF corresponding to the in-situ resistance measurements of the un-biased DUTs, whereas the bottom row shows the time-to-failure corresponding to the in-situ voltage measurements of the biased DUTs. Each step increase/decrease in the measurements indicates a DUT failure. As seen from the measurement results, the step changes (i.e. the failures), whether biased or unbiased, occur at similar times for each DUT type. Therefore, no differences in the time-to-failures probability could be observed, indicating that voltage biasing has little to no influence on the failure mechanism.

It is noted that in the biased experiment, once a DUT fails into an open circuit, the applied stress voltage over the remaining parallel connected DUTs increases slightly (and, as a result, the voltage over the reference resistor drops slightly). The maximum added stress voltage remains within 1.5% of the rated voltage of the DUTs and is assumed to have a negligible effect on the resistors.

Table 4 presents the obtained values from the Weibull probability distribution. The parameter β for all vendors shows that the failure rate is increasing ($\beta > 1$) and results in a wear out failure due to corrosion for the DUTs. In Weibull analysis, parameter η describes the time at which 63.2% of the thick film resistors have failed. N presents the amount of failures in each experiment and AD is the Anderson-Darling (AD) statistic, which measures how well the data follows the Weibull distribution. The p-value determinates whether the data follows a normal distribution. Because the p-values for all vendors was greater than the significance level of 0.05, the decision was not to reject the null hypothesis and it cannot be concluded that the data does not follow a normal distribution.

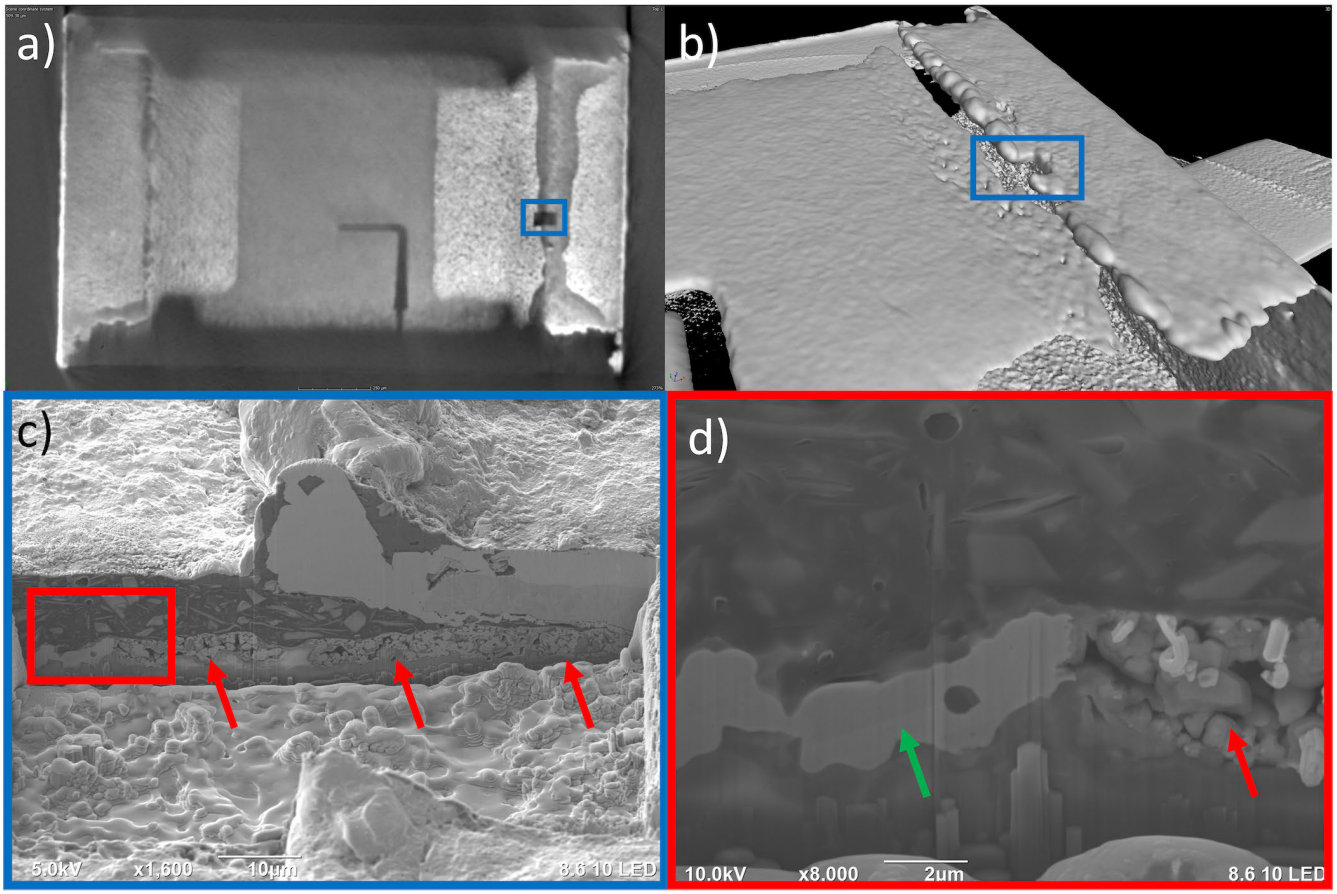

FIGURE 11. 3D X-ray images of a failed thick film resistor (vendor E) and location of the FIB cut (blue box) are depicted in a) and b). c) shows the corrosion product observed with FIB and d) shows the interface between the pure and corroded silver electrode.

Comparing DUT type H and E, both having similar end termination structures and conformal epoxy thicknesses, indicates an approximately ten-time higher η for the H type. Likewise, comparing DUT type F with G and I, all having similar conformal epoxy thickness at the end termination, indicates an approximate a four-time higher η for type F. Thus, based on the results, no direct correlation between the structure of the conformal epoxy layer and TTF in the corrosion experiments could be drawn. No failures were observed in the reference DUTs type B with anti-sulphur packaging.

X-ray images of an un-biased and a biased DUT taken before and after the FOS experiment are shown in Fig. 8. Fig. 8b) and d), both taken after the experiment of an unbiased and a biased DUT respectively, clearly shows severe corrosion of the underlying silver electrode resulting in open contacts. The corroded area is indicated by orange arrows. Shown in the obtained X-ray images, the unbiased and biased DUTs have failed due to the same corrosion failure mechanism. Together with the results from the time-to-failure data, it can be concluded that the voltage bias has negligible influence on the corrosion mechanism in thick film resistors failing in an open connection. Approximately 60% of the DUTs failed in an open connection and all were detected with 2D X-ray imaging. Furthermore, the progression of the corrosion was observed to be similar for all suppliers.

A sequence of X-ray images, taken at 0 hour until the open connection of the thick film resistor in the FOS experiment is shown in Fig. 9 and the corresponding online resistance measurements of the same DUT is shown in Fig. 10. The first sign of corrosion in the underlying silver layer is observed already at 24 hours in the X-ray image, even though no changes in the electrical measurements were observed. The corroded location is indicated by a red box in Fig. 9. The corrosion is seen as a small white area in the middle of the right-hand side end termination. Moreover, a denser material had appeared at the end of the end termination (seen as a black dot). After 36 hours, the propagation of the corrosion was easily observed as a bright stripe at the underlying silver layer, covering almost the full length of the end termination. Additionally, a dark line of denser material was now observed at the end of the top metallization. After 48 hours, only a small electrical connection remains, shown as a green arrow in Fig. 9. The only change in the electrical measurement was observed after 57 hours as the resistor failed in an open circuit indicated as a large step increase in the measured resistance shown in Fig. 10. In the following X-ray image

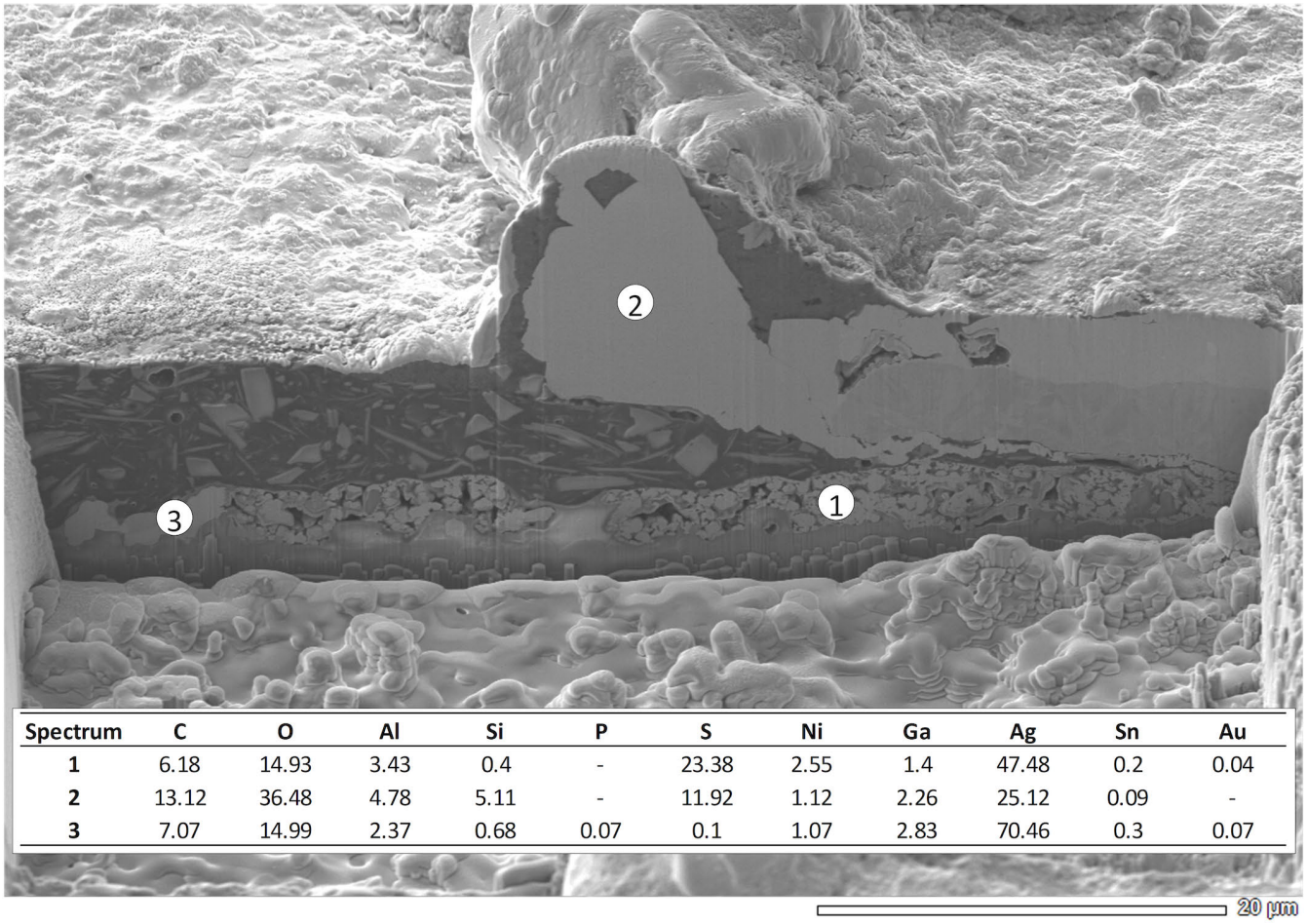

Spectrum	C	O	Al	Si	P	S	Ni	Ga	Ag	Sn	Au
1	6.18	14.93	3.43	0.4	-	23.38	2.55	1.4	47.48	0.2	0.04
2	13.12	36.48	4.78	5.11	-	11.92	1.12	2.26	25.12	0.09	-
3	7.07	14.99	2.37	0.68	0.07	0.1	1.07	2.83	70.46	0.3	0.07

FIGURE 12. EDX point scan locations.

taken at 60 hours, a large area of the underlying silver layer had completely corroded.

To verify the results observed with the 2D X-ray imaging technique, a μ-computerized tomography X-ray image of the failed DUT was taken and compared with results obtained with FIB of the same DUT. The FIB cut at the end of the top metallization of the end termination is indicated by the blue box in the μ-CT X-ray image Fig. 11a) and b). As seen in the FIB image c) the underlying silver electrode has transformed into a porous corrosion product causing a change in the material density which can be detected with 2D X-ray imaging. The transition area of the porous corrosion product (red arrows) to the non-corroded silver layer (green arrow) is shown Fig. 11d) which corresponds to the red box in Fig. 11c). Additionally, multiple-point EDX scans were taken from the FIB cut with the corresponding atomic percentage of each element at the points shown in Fig. 12. Based on the EDX results, the elemental ratios at the corrosion location in point 1 is roughly 2:1, indicating that the underlying silver electrode has formed into silver sulphide by the reaction

$$2\mathrm{Ag} + \mathrm{S}^{2-} \rightarrow \mathrm{Ag_2S} + 2e^{-}(s). \tag{7}$$

The protrusion at point 2 in the EDX measurements consists of silver sulphide which has originated from the underlying silver electrode. This protrusion phenomenon is caused by forces created by volumetric expansion of the corrosion product, which ''pushes'' the growth out from the interface between the conformal organic epoxy layer and the top metallization. This same protrusion was observed as a dark line of denser material at the end of the top metallization in the 2D X-ray images. Finally, point 3 shows the elemental analysis results at the un-corroded silver electrode.

In the single gas experiment, no increase or decrease in the electrical measurements were observed as shown in Fig. 13. Fig. 13a) presents the in-situ resistance measurements of the un-biased DUTs, whereas Fig. 13b) shows the in-situ voltage measurements of the biased DUTs. Although, no failures were observed in the electrical measurements, incipient corrosion was detected in multiple DUTs with 2D X-ray imaging. In Fig. 14, the red arrows depict the incipient corrosion in two thick film resistors from different vendors. The bright area at the end termination reveals the corrosion in the underlying silver electrode.

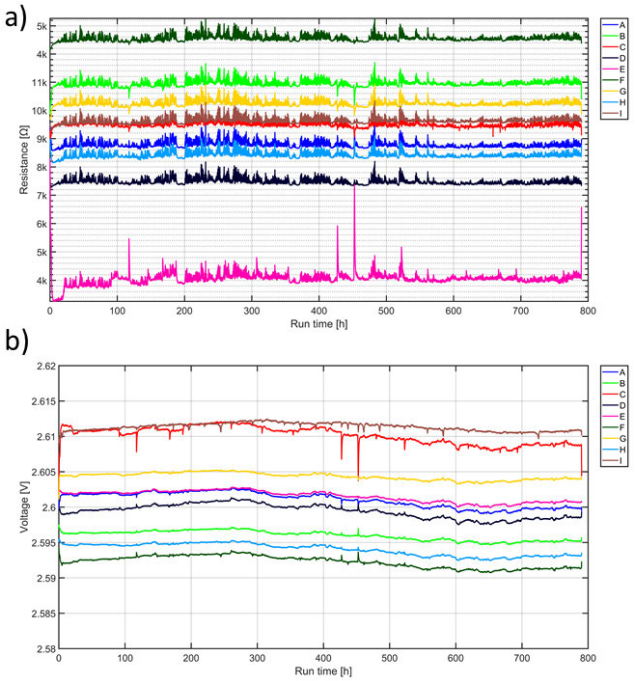

FIGURE 13. In-situ resistance and voltage measurements obtained from the single gas unbiased and biased experiments, respectively.

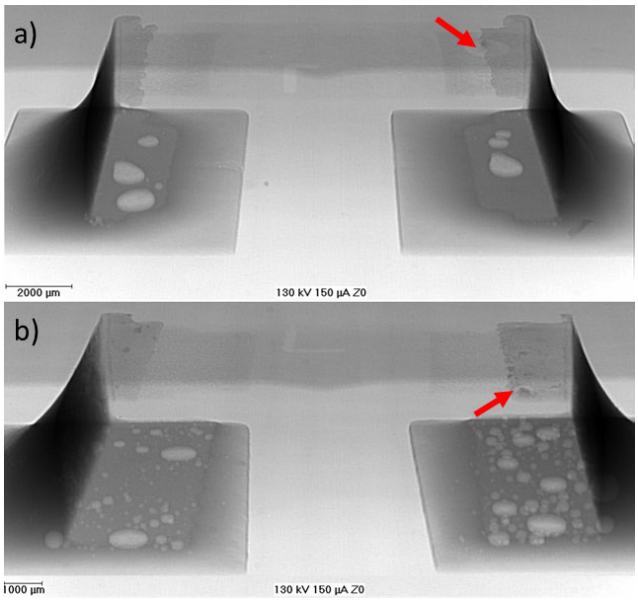

FIGURE 14. 2D X-ray images showing incipient corrosion in DUTs from the single gas experiment (top: vendor G and bottom: vendor I).

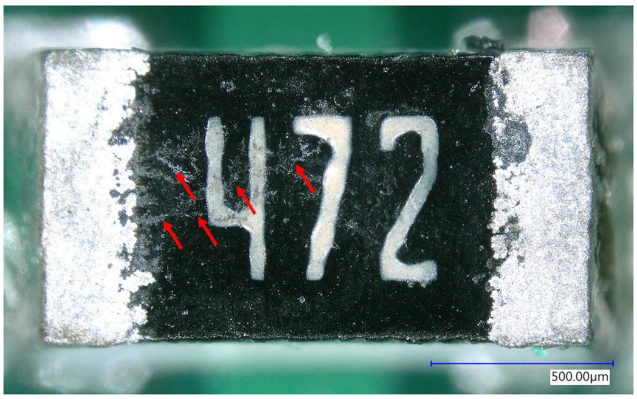

FIGURE 15. The red arrows depict the electrochemical corrosion on top of the conformal epoxy layer (vendor H).

On the other hand, in the biased single gas experiment an additional electrochemical corrosion failure mechanism was observed where the sulphur gas initiates silver dendrite growth on top of the conformal organic epoxy between the end terminals of the tick film resistors, as shown in Fig. 15.

IV. DISCUSSION

Two different corrosion experiments were used to produce corrosion in thick film resistors. In both the FOS and single gas experiments, corrosion of the silver electrodes was observed. In the FOS experiment, the corrosion resulted in most DUTs failing in an open circuit during the 750-hour test time, whereas, in the single gas experiment, no open circuit failures could be observed during the experiment. Although no failures were recorded in the electrical measurements for the single gas experiment, incipient corrosion in the silver electrode was still detected with 2D X-ray imaging. The Ag_2S corrosion product observed in the DUTs was verified with FIB and the corrosion observed in the X-ray imaging corresponded well to the obtained results from the SEM image and the elemental analysis.

Both experiments are standardized, with only minor changes made to the temperature and humidity for the single gas experiment to accelerate the corrosion, only the FOS experiment was found to be applicable for a thick film resistor corrosion resistance evaluation in a practical testing time. The main reason for the different time-to-failure results is that the flowers of sulphur experiment is extremely aggressive, as shown in a comparison between single gas and flowers of sulphur setups in Ostermans *et al.* work [25]. In their work, it was shown that the corrosion thickness (nm/day) in copper coupons for a single gas experiment when using 1.8 ppm H_2S was 163.2 nm/day and in the flowers of sulphur experiment, 54094.2 nm/day. In our study, the amount of H_2S gas (15 ppm) in the single gas experiment was still too low and the test time was too short to obtain equivalent results as in the flowers of sulphur experiment. However, the single gas experiment should not be dismissed completely, as a biased single gas experiment with a higher humidity and H_2S gas concentration enables a reliable evaluation of thick film resistors in terms of resistance to electrochemical corrosion, as was shown in Fig. 15. In this case, X-ray imaging is not needed as the silver dendrite growth is optically observable.

Two major results were obtained in this study. Firstly, this paper clearly shows that 2D X-ray imaging is a powerful imaging technique for observing corrosion in thick film resistors. Contrary to most used methods for evaluating the

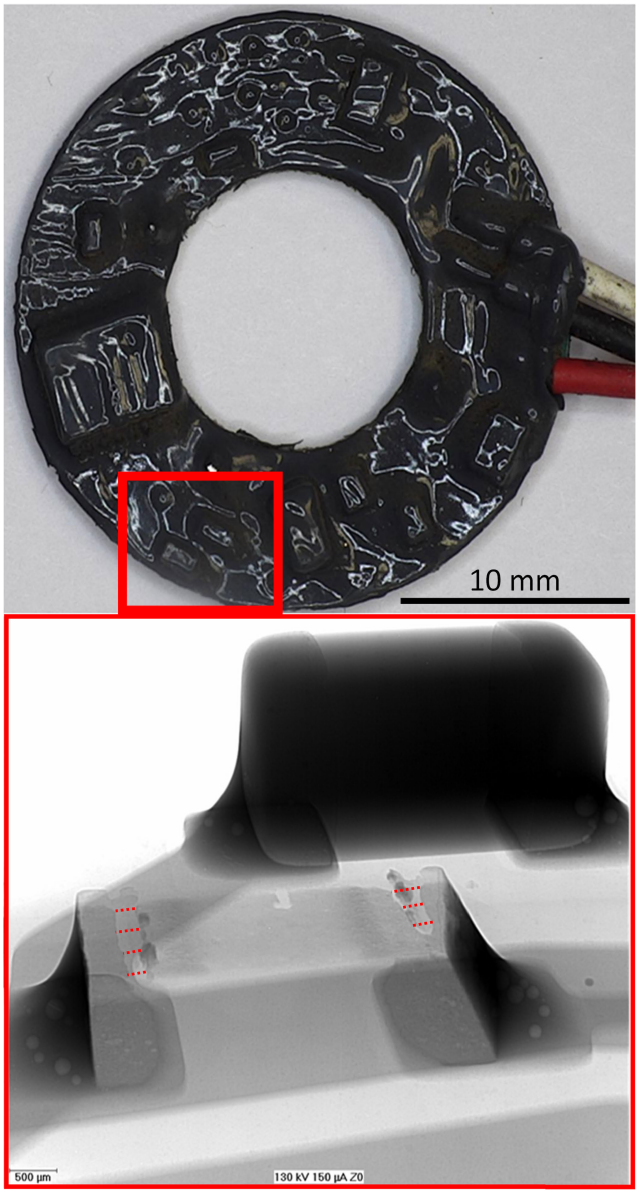

FIGURE 16. A failed device, where a corroded thick film resistor caused a critical process to stop. The corrosion can be observed in the 2D X-ray image shown with red dotted lines.

corrosion failures in thick film resistors, this technique can be used without destroying the printed circuit board assembly or single component. Furthermore, X- ray imaging was found to be a unique method for investigating the corrosion propagation in thick film resistors. From Fig. 9 and Fig. 10, it can be concluded that the change in resistance takes place instantaneously at the end of the corrosion propagation when the last contact point at either terminal finally corrodes open.

Secondly, the applied voltage bias of 7.5 V over the DUTs did not accelerate the corrosion. When comparing the results from the time-to-failure data, it can be concluded that the voltage bias has negligible influence on the corrosion mechanism in thick film resistors when failing in open connection. Furthermore, the failure signature from both biased and unbiased experiments showed identical corrosion progression, as shown in Fig. 8.

As an additional note, the failure mechanism produced in the corrosion experiments corresponds well to failures observed in the field where a device or a system has been exposed to a sulphuric atmosphere. Fig. 16 shows a device where a corroded thick film resistor caused a critical process to stop. As seen from Fig. 16, an open connection in the underlying silver electrode was easily observed with 2D X-ray imaging. The corroded area is shown with red dotted lines in the figure. Without X-ray imaging, it would not be possible to identify the root cause of the failure due to the black potting material on top of the surface mounted devices (SMD) of the failed device.

V. CONCLUSION

Two setups, a single gas and a flowers of sulphur experiment, were realized for evaluating corrosion progression in thick film resistors. The propagation of the corrosion was successfully examined by the implemented 2D X-ray imaging technique. FIB and EDX analysis were further utilized to verify the observed corrosion product.

In the single gas test, only incipient corrosion of the silver electrodes could be detected in the DUTs. However, optical analysis revealed an additional electrochemical corrosion failure mechanism in the form of dendrite growth on top of the conformal organic epoxy layer of the resistors.

In the FOS experiment, severe corrosion of the silver electrodes was observed in most of the DUTs. The corrosion occurred and progressed similarly, whether a voltage bias was applied over the DUTs or not. Hence, care must be taken when storing commercial thick film resistors, as exposure to a sulphuric environment may cause the eventual electrical device (end product) to fail already during commissioning.

In this study, the 2D X-ray imaging technique was successfully implemented to observe corrosion propagation in thick film resistors. This novel technique enables a fast and non-destructive investigation of corrosion in thick film resistors, as well as providing additional crucial information for further in-depth failure analysis. Moreover, for thick film resistor benchmarking and reliability assessment, this technique allows for a quick evaluation of the protective coating applied on thick film resistors. For thick film resistor benchmarking, only the flowers of sulphur experiment proved to be successful, and the resulting failure signature was found to correspond well with failed thick film resistors exposed to a sulphuric environment in the field.

REFERENCES

[1] T. N. Wassermann, O. Schilling, K. Müller, A. Rossin, and J. Uhlig, "A new high-voltage H_2S single noxious gas reliability test for power modules," *Microelectron. Rel.*, vols. 100–101, Sep. 2019, Art. no. 113468, doi: 10.1016/j.microrel.2019.113468.

[2] C. F. Bayer, A. Diepgen, T. Filippi, C. Fuchs, S. Wustefeld, S. Kellner, U. Waltrich, and A. Schletz, "Electrochemical corrosion on ceramic substrates for power electronics—Causes, phenomenological description, and outlook," in *Proc. 10th Int. Conf. Integr. Power Electron. Syst. (CIPS)*, Stuttgart, Germany, 2018, pp. 161–167.

[3] D. Minzari, M. S. Jellesen, P. Moller, P. Wahlberg, and R. Ambat, "Electrochemical migration on electronic chip resistors in chloride environments," *IEEE Trans. Device Mater. Rel.*, vol. 9, no. 3, pp. 392–402, Sep. 2009, doi: 10.1109/TDMR.2009.2022631.

[4] C. Hillman, J. Arnold, S. Binfield, and J. Seppi, "Silver and sulfur: Case studies, physics, and possible solutions," in *Proc. SMTA Int. Conf.*, 200, pp. 1–13.

[5] Rockwell Automation, Milwaukee, WI, USA. (2009). *Corrosion Resistance of Electric Wire Terminals Used in Harsh Industrial Environments*. Accessed: May 27, 2021. [Online]. Available: https://literature.rockwellautomation.com/idc/groups/literature/documents/wp/1492-wp003_-en-p.pdf

[6] M. Watanabe, A. Hokazono, T. Handa, T. Ichino, and N. Kuwaki, "Corrosion of copper and silver plates by volcanic gases," *Corrosion Sci.*, vol. 48, no. 11, pp. 3759–3766, Nov. 2006, doi: 10.1016/j.corsci.2005.12.009.

[7] H. Kim, "Corrosion process of silver in environments containing 0.1 ppm H_2S and 1.2 ppm NO_2," *Mater. Corrosion*, vol. 54, no. 4, pp. 243–250, Apr. 2003, doi: 10.1002/maco.200390053.

[8] T. E. Graedel, J. P. Franey, G. J. Gualtieri, G. W. Kammlott, and D. L. Malm, "On the mechanism of silver and copper sulfidation by atmospheric H_2S and OCS," *Corrosion Sci.*, vol. 25, no. 12, pp. 1163–1180, Dec. 1985, doi: 10.1016/0010-938X(85)90060-5.

[9] M. Reid, M. N. Collins, E. Dalton, J. Punch, and D. A. Tanner, "Testing method for measuring corrosion resistance of surface Mount chip resistors," *Microelectron. Rel.*, vol. 52, no. 7, pp. 1420–1427, Jul. 2012, doi: 10.1016/j.microrel.2012.02.020.

[10] M. Reid, J. Punch, C. Ryan, J. Franey, G. E. Derkits, W. D. Reents, and L. F. Garfias, "The corrosion of electronic resistors," *IEEE Trans. Compon. Packag. Technol.*, vol. 30, no. 4, pp. 666–672, Dec. 2007, doi: 10.1109/TCAPT.2007.901749.

[11] M. Cole, L. Hedlund, G. Hutt, T. Kiraly, L. Klein, S. Nickel, P. Singh, and T. Tofil, "Harsh environment impact on resistor reliability," in *Proc. SMTA Int. Conf.*, Orlando, FL, USA, 2010, pp. 1–9.

[12] M. Cole, J. Porter, J. Wertz, M. Coq, J. Wilcox, and M. Meilunas, "Effectiveness of conformal coatings in preventing resistor silver sulfide corrosion," in *Proc. SMTA Int. Conf.*, Rosemont, IL, USA, 2016, pp. 937–944.

[13] P. Singh, L. Palmer, H. Fu, D. Lee, J. Lee, K. Guo, J. Li, S. Lee, G. Tong, and C. Xu, "A flowers of sulfur corrosion chamber for testing electronic hardware," in *Proc. Pan Pacific Microelectron. Symp.*, Big Island, HI, USA, Feb. 2018, pp. 1–10.

[14] *Environmental Testing—Part 2–43: Tests—Test Kd: Hydrogen Sulphide Test for Contacts and Connections*, Standard IEC 60068-2-43, 2005.

[15] *Environmental Testing—Part 2–42: Tests—Test Kc: Sulphur Dioxide Test for Contacts and Connections*, Standard IEC 60068-2-42, 2005.

[16] K. Eguchi, T. L. Burnett, and D. L. Engelberg, "X-ray tomographic characterisation of pitting corrosion in lean duplex stainless steel," *Corrosion Sci.*, vol. 165, Apr. 2020, Art. no. 108406, doi: 10.1016/j.corsci.2019.108406.

[17] S. M. Ghahari, A. J. Davenport, T. Rayment, T. Suter, J.-P. Tinnes, C. Padovani, J. A. Hammons, M. Stampanoni, F. Marone, and R. Mokso, "*In situ* synchrotron X-ray micro-tomography study of pitting corrosion in stainless steel," *Corrosion Sci.*, vol. 53, no. 9, pp. 2684–2687, Sep. 2011, doi: 10.1016/j.corsci.2011.05.040.

[18] A. Česen, T. Kosec, and A. Legat, "Characterization of steel corrosion in mortar by various electrochemical and physical techniques," *Corrosion Sci.*, vol. 75, pp. 47–57, Oct. 2013, doi: 10.1016/j.corsci.2013.05.015.

[19] P.-A. Itty, M. Serdar, C. Meral, D. Parkinson, A. A. MacDowell, D. Bjegović, and P. J. M. Monteiro, "*In situ* 3D monitoring of corrosion on carbon steel and ferritic stainless steel embedded in cement paste," *Corrosion Sci.*, vol. 83, pp. 409–418, Jun. 2014, doi: 10.1016/j.corsci.2014.03.010.

[20] C. Wang, Y. Hua, S. Nadimi, W. Taleb, R. Barker, Y. Li, X. Chen, and A. Neville, "Determination of thickness and air-void distribution within the iron carbonate layers using X-ray computed tomography," *Corrosion Sci.*, vol. 179, Feb. 2021, Art. no. 109153, doi: 10.1016/j.corsci.2020.109153.

[21] *Test Method—Electronic Passive Components Exposure to Atmospheric Sulfur*, Standard EIA-977, 2017.

[22] F. P. Incropera and D. P. De Witt, *Fundamentals of Heat and Mass Transfer*, 3rd ed. New York, NY, USA: Wiley, 1990.

[23] Direct Industry. (2021). *nanome|x—The High-End 2D and 3D X-Ray Solution*. Accessed: May 27, 2021. [Online]. Available: https://pdf.directindustry.com/pdf/inspection-technologies/nanomex/9257-365093.html

[24] J. M. Ingman, J. P. A. Jormanainen, A. M. Vulli, J. D. Ingman, K. Maula, T. J. Kärkkäinen, and P. Silventoinen, "Localization of dielectric breakdown defects in multilayer ceramic capacitors using 3D X-ray imaging," *J. Eur. Ceram. Soc.*, vol. 39, no. 4, pp. 1178–1185, Apr. 2019, doi: 10.1016/j.jeurceramsoc.2018.10.030.

[25] M. Osterman. (Apr. 30, 2015). Corrosion concerns and testing for electronic equipment. University of Maryland, Collage Park, MD, USA. Accessed: May 27, 2021. [Online]. Available: http://thor.inemi.org/webdownload/2015/Corrosion_Concerns_043015.pdf

JONNY M. INGMAN (Graduate Student Member, IEEE) was born in Kerava, Finland, in 1989. He received the B.Sc. and M.Sc. degrees in mechanical engineering from Aalto University, Espoo, Finland, in 2013 and 2015, respectively. He is currently pursuing the Ph.D. degree in energy systems with Lappeenranta University of Technology (LUT), Lappeenranta, Finland.

He is also working as a Senior Reliability Engineer at ABB Drives Oy, Helsinki, Finland. His research interest includes physics of failure in electronics and power electronics.

JONI P. A. JORMANAINEN was born in Tammisaari, Finland, in 1986. He received the M.Sc. degree in electronics and electrical engineering from Aalto University, Espoo, Uusimaa, Finland, in 2017.

He is currently working at ABB Drives Oy, Helsinki, Finland. His research interest includes reliability of power electronics.

SAMU K. JÄRVINEN was born in Helsinki, Finland, in 1992. He received the B.Sc. degree in electronics and electricity and the M.Sc. degree in electronics and nanotechnology from Aalto University, Espoo, Finland, in 2017 and 2020, respectively.

He is currently a Quality and Reliability Engineer at ABB Drives Oy, Helsinki.

NATALIA I. KANKO was born in Tampere, Finland, in 1992. She received the B.Sc. degree in electrical engineering from Tampere University, Finland, in 2020.

She is currently a Student of electrical engineering with Tampere University. She is also working as a Failure Analysis Engineer at ABB Drives Oy, Helsinki, Finland.

JOONAS A. R. LEPPÄNEN was born in Helsinki, Finland, in 1990. He received the B.Sc. and M.Sc. degrees majoring in micro- and nanoscience from the School of Electrical Engineering, Aalto University, Finland, in 2017. He is currently pursuing the Ph.D. degree with Aalto University and ABB.

From 2013 to 2015, he worked as a Laboratory Engineer, focusing on failure analysis at ABB Drives. In 2015, he continued as a Reliability Engineer at ABB Drives while simultaneously completing his master's thesis, titled 'Humidity Induced Failure Mechanisms in Power Semiconductor Devices' used in power converters. From 2017 to 2019, he worked as a Reliability Engineer at ABB Solar, focusing on the development of solar inverters. He is currently a Senior Design Engineer in semiconductors at ABB Drives Oy, Helsinki, he is responsible for the quality and reliability of the power semiconductor devices used in power converters.

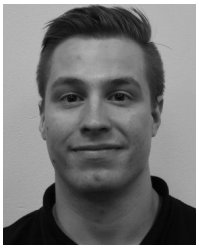

ALEKSI M. VULLI was born in Vantaa, Finland, in 1989. He received the M.Sc. (Tech.) degree in control, robotics and autonomous systems from the School of Electrical Engineering, Aalto University, Espoo, Finland, in 2018. He is currently pursuing the Ph.D. degree in prognostics in electric drives from Aalto University and ABB, Helsinki, Finland. He completed his master's thesis with the title of 'Accelerated Ageing and Prognostics of Silicon Carbide Power MOSFET.'

From 2019 to 2021, he acted as a Manager in a research project for prognostics in electric drives, while also working as a Scientist in the project, studying mathematical methods for prognosis. He is also a Reliability Engineer at ABB Drives Oy, he is responsible for designing and implementing autonomous reliability test systems for various drive components, as well as analyzing collected data to construct lifetime models.

TOMMI J. KÄRKKÄINEN (Member, IEEE) was born in Finland, in 1987. He received the B.Sc., M.Sc., and D.Sc. degrees from Lappeenranta University of Technology (LUT), Lappeenranta, Finland, in 2010, 2011, and 2015, respectively.

He is currently a Postdoctoral Researcher with LUT School of Energy Systems. His main research interests include reliability of power electronic devices and systems, and the utilization of machine learning algorithms to improve the reliability and productivity of various systems.

JUUSO RAUTIO (Member, IEEE) was born in Lappeenranta, Finland, in 1993. He received the B.Sc. and M.Sc. degrees from LUT University, in 2015 and 2018, respectively. He is currently pursuing the Ph.D. degree in reliability of power electronic components and devices in corrosive environments with LUT School of Energy Systems.

He is also a Junior Researcher with LUT School of Energy Systems.

JANNE JÄPPINEN (Member, IEEE) was born in Imatra, Finland, in 1993. He received the B.Sc. and M.Sc. degrees from LUT University, in 2017 and 2019, respectively, where he is currently pursuing the Ph.D. degree in reliability and chemical corrosion of electronics with the Laboratory of Applied Electronics.

He is also a Junior Researcher with the Laboratory of Applied Electronics, LUT University.

PERTTI SILVENTOINEN (Member, IEEE) was born in Simpele, Finland, in 1965. He received the M.Sc. degree in electrical engineering, the Licentiate of Technology degree in applied electronics and control systems, and the D.Sc. degree with the focus on EMC in electronics from Lappeenranta University of Technology Finland (LUT University), in 1993, 1997, and 2001, respectively. Since 2008, he has been a Full Professor of applied electronics with LUT University. His research interests include analog signal processing and measurement systems, power line communication applications, EMC measurement technology, and power electronic systems in various forms.